J. Plasma Physics (2002), *vol.* 67, *part* 1, *pp.* 27–47.
DOI: 10.1017/S0022377801001313 Printed in the United Kingdom

A transient Hartmann flow with heat transfer of a non-Newtonian fluid with suction and injection, considering the Hall effect

HAZEM ALI ATTIA[1,2]
and MOHAMED EISSA SAYED-AHMED[1]

[1]Department of Engineering Mathematics and Physics, Faculty of Engineering, Cairo University (El-Fayoum Branch), Egypt

[2]Current address: Department of Mathematics, College of Science, King Saud University (Al-Qasseem Branch), PO 237, Buraidah 81999, Kingdom of Saudi Arabia

(Received 24 October 2000)

Abstract. The transient Hartmann flow of an electrically conducting viscous incompressible non-Newtonian power-law fluid between two parallel horizontal non-conducting porous plates is studied with heat transfer, without neglecting the Hall effect. A sudden uniform and constant pressure gradient, an external uniform magnetic field that is perpendicular to the plates, and uniform suction and injection through the surface of the plates are applied. The two plates are kept at different but constant temperatures, while the Joule and viscous dissipations are taken into consideration. Numerical solutions for the governing nonlinear momentum and energy equations are obtained using finite difference approximations. The effect of the Hall term, the parameter describing the non-Newtonian behavior, and the velocity of suction and injection on both the velocity and temperature distributions as well as the dissipation terms are examined.

1. Introduction

The study of the rectangular channel flow of an electrically conducting viscous fluid under the action of a transversely applied magnetic field, known as Hartmann flow, has immediate applications in many devices such as magnetohydrodynamic (MHD) power generators, MHD pumps, accelerators, aerodynamic heating, electrostatic precipitation, polymer technology, the petroleum industry, purification of crude oil and fluid droplets and sprays. Channel flows of a Newtonian fluid with heat transfer have been studied, with or without Hall currents, by many authors (Tao 1960; Nigam and Singh 1960; Alpher 1961; Tani 1962; Sutton and Sherman 1965; Soundalgekar et al. 1979; Soundalgekar and Uplekar 1986; Attia and Kotb 1996; Attia 1998). These results are important for the design of duct walls and cooling arrangements.

A number of industrially important fluids, such as molten plastics, polymers, pulps, and foods exhibits non-Newtonian fluid behavior (Nakayama and Koyama 1988). Due to the growing use of these non-Newtonian materials in various manufacturing and processing industries, considerable effort has been directed towards understanding their flow and heat transfer characteristics. Many of the inelastic

non-Newtonian fluids encountered in chemical engineering processes are known to follow the so-called 'power-law model' in which the shear stress varies according to a power function of the strain rate (Metzner 1965). The power-law fluid flows, within parallel-plate ducts and rectangular ducts, have been considered by many authors (Tien 1962; Gao and Hartnett 1992; Ibrahim and Terbeche 1994; Patel and Ingham 1994).

Attia (1998) has studied the influence of the Hall current on the velocity and temperature fields of the unsteady Hartmann flow of a conducting Newtonian fully developed fluid between two infinite non-conducting horizontal parallel and porous plates. The extension of such problem to the case of a non-Newtonian power-law fluid is made in the present study. The flow starts from rest through the application of a uniform and constant pressure gradient and a uniform suction from above and a uniform injection from below, and is subjected to a uniform magnetic field perpendicular to the plates. The Hall current is taken into consideration, while the induced magnetic field is neglected by assuming a very small magnetic Reynolds number (Sutton and Sherman 1965). The two plates are kept at two different but constant temperatures. This configuration is a good approximation to some practical situations such as heat exchangers, flow meters, and pipes that connect system components. The Joule and viscous dissipations are taken into consideration in the energy equation. The governing nonlinear momentum and energy equations are solved numerically using finite difference approximations. The inclusion of the Hall current as well as the non-Newtonian fluid characteristics leads to some interesting effects on both the velocity and temperature fields.

2. Formulation of the problem

The geometry of the problem is shown in Fig. 1. The fluid is assumed to be laminar, viscous and incompressible, and to obey the power-law model, and is assumed to flow between two infinite horizontal parallel non-conducting plates located at the $y = \pm h$ planes and extending from $x = 0$ to ∞ and from $z = 0$ to ∞. The upper and lower plates are kept at two constant temperatures T_2 and T_1, respectively, with $T_2 > T_1$. The flow is driven by a uniform and constant pressure gradient dp/dx in the x direction, and a uniform suction from above and injection from below, which are applied at $t = 0$. A uniform magnetic field with magnetic flux density vector $\mathbf{B}_0$ is applied in the positive y direction. The Hall effect is taken into consideration, and consequently a z component of the velocity is expected to arise. The uniform suction implies that the y component of the velocity is constant. Thus, the velocity vector of the fluid is given by

$$\mathbf{v}(y, t) = u(y, t)\mathbf{i} + v_0\mathbf{j} + w(y, t)\mathbf{k}.$$

It should be noted that the problem turns out to be linear. In the hydrodynamic case without suction–injection, the problem reduces to the Poiseuille problem (Schlichting 1968) – the classical hydrodynamic linear problem. Without suction–injection and neglecting the Hall current, it reduces to the Hartmann–Poiseuille problem (Crammer and Pai 1973) – the classical MHD linear problem. The inclusion of the constant suction–injection as well as the Hall term (Attia 1998) preserves linearity – so obviously does changing the Newtonian fluid to a non-Newtonian one in the present study. The classical problems (Poiseuille and Hartmann–Poiseuille) of channel flow and the related pipe flow of a Newtonian fluid are known to be

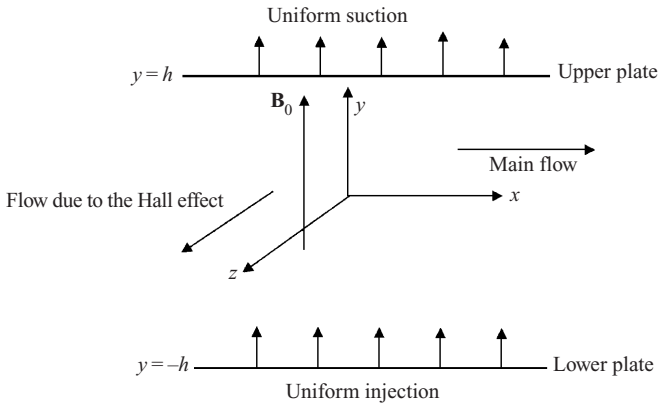

Figure 1. The geometry of the problem.

attainable in practice and to give results in excellent agreement with experiments. The fully developed profiles are observed away from the inlet and the sidewalls of the channel. Using a non-Newtonian fluid is not expected to cause a problem.

The fluid motion starts from rest at $t = 0$, and the no-slip condition at the plates implies that the fluid velocity has neither a z nor an x component at $y = \pm h$. The initial temperature of the fluid is assumed to be equal to T_1. As in the classical problems (Poiseuille and Hartmann–Poiseuille), it is assumed that the separation between the two plates is small in comparison with the length of the channel (Schlichting 1968; Crammer and Pai 1973). Consequently the endwall effect can be neglected, and the plates are assumed to be infinite in the x and z directions, which means that the physical quantities do not change in these directions.

The flow of the fluid is governed by the Navier–Stokes equation (Schlichting 1968; Kakac et al. 1987)

$$\rho \frac{D\mathbf{v}}{Dt} = \boldsymbol{\nabla} \cdot (\mu \boldsymbol{\nabla} \mathbf{v}) - \boldsymbol{\nabla} p + \mathbf{J} \times \mathbf{B}_0, \tag{1}$$

where ρ is the density of the fluid and μ is the apparent viscosity of the model, and is given by

$$\mu = K \left[\left(\frac{\partial u}{\partial y} \right)^2 + \left(\frac{\partial w}{\partial y} \right)^2 \right]^{(n-1)/2}, \tag{2}$$

where K is the consistency index, n is the flow behavior index (which corresponds to the type of fluid: $n < 1$, $n = 1$, and $n > 1$ give pseudoplastic, Newtonian, and dilatant fluids respectively), and $\mathbf{B}_0$ is the magnetic field, which is assumed to be also the total magnetic field, since the induced magnetic field is neglected by assuming a very small magnetic Reynolds number (Sutton and Sherman 1965). Assuming that there is no excess charge density, $\boldsymbol{\nabla} \cdot \mathbf{E} = 0$, where $\mathbf{E}$ is the induced electric field. Since the magnetic Reynolds number is very small, the induced magnetic field and consequently $\boldsymbol{\nabla} \times \mathbf{E}$ are negligible, which, in conjuction with the result $\boldsymbol{\nabla} \cdot \mathbf{E} = 0$, shows that the induced electric field can be ignored (Sutton and Sherman 1965; Crammer and Pai 1973). For small and moderate values of the magnetic field, the Hall term may be ignored in applying Ohm's law, since it has no marked effect. However, the current trend in the application of MHD is towards a strong magnetic field, so that the influence of the electromagnetic force is noticeable (Crammer and

https://doi.org/10.1017/S0022377801001313 Published online by Cambridge University Press

Pai 1973). Under these conditions, the Hall current is important, and has a marked effect on the magnitude and direction of the current density and consequently on the magnetic force term. If the Hall term is retained, the current density **J** is given by

$$\mathbf{J} = \sigma[\mathbf{v} \times \mathbf{B}_0 - \beta(\mathbf{J} \times \mathbf{B}_0)], \tag{3}$$

where σ is the electric conductivity of the fluid and β is the Hall factor (Sutton and Sherman 1965). Equation (3) may be solved in **J** to yield

$$\mathbf{J} \times \mathbf{B}_0 = -\frac{\sigma B_0^2}{1+m^2}[(u+mw)\mathbf{i} + (w-mu)\mathbf{k}], \tag{4}$$

where $m = \sigma\beta B_0$ is the Hall parameter. Thus, the two components of the Navier–Stokes equation (1) read

$$\rho\frac{\partial u}{\partial t} + \rho v_0\frac{\partial u}{\partial y} = -\frac{dp}{dx} + \frac{\partial}{\partial y}\left(\mu\frac{\partial u}{\partial y}\right) - \frac{\sigma B_0^2}{1+m^2}(u+mw), \tag{5}$$

$$\rho\frac{\partial w}{\partial t} + \rho v_0\frac{\partial w}{\partial y} = \frac{\partial}{\partial y}\left(\mu\frac{\partial w}{\partial y}\right) - \frac{\sigma B_0^2}{1+m^2}(w-mu). \tag{6}$$

The energy equation with viscous and Joule dissipations is given by

$$\rho c_p\frac{\partial T}{\partial t} + \rho c_p v_0\frac{\partial T}{\partial y} = k\frac{\partial^2 T}{\partial y^2} + \mu\left[\left(\frac{\partial u}{\partial y}\right)^2 + \left(\frac{\partial w}{\partial y}\right)^2\right] + \frac{\sigma B_0^2}{1+m^2}(u^2+w^2), \tag{7}$$

where c_p and k are, respectively, the specific heat capacity at constant volume and the thermal conductivity of the fluid. The second and third terms on the right-hand side represent the viscous and Joule dissipations, respectively. We notice that each of these terms has two components. This is because the Hall effect brings about a velocity w in the z direction. The viscous dissipation term may often be neglected for Newtonian fluids; however, depending on the duct geometry and the relative volumetric flow rate, viscous dissipation may have a dramatic effect on the thermal flow field in non-Newtonian fluids (Gingrich et al. 1992).

The initial and boundary conditions of the problem are given by

$$u = w = 0 \quad \text{at } t \leqslant 0; \qquad u = w = 0 \quad \text{at } y = \pm h \quad \text{for } t > 0; \tag{8}$$

$$T = T_1 \quad \text{at } t \leqslant 0; \qquad T = T_2 \quad \text{at } y = h \quad \text{and} \quad T = T_1 \quad \text{at } y = -h \quad \text{for } t > 0. \tag{9}$$

That the boundary conditions do not show any dependence on x suggests that the problem has a fully developed solution of the form

$$u = u(y,t), \qquad v = v_0, \qquad p = P + Gx,$$

where P is the pressure at $x = 0$ (constant) and G is the constant pressure gradient (negative). Under these conditions, the continuity equation $\partial u/\partial x + \partial v/\partial y = 0$ is automatically satisfied.

It is expedient to write the above equations in non-dimensional form. To do this, we introduce the following non-dimensional quantities:

$$\bar{x} = \frac{x}{h}, \quad \bar{y} = \frac{y}{h}, \quad \bar{z} = \frac{z}{h}, \quad \bar{t} = \frac{tu_0}{h}, \quad \bar{u} = \frac{u}{u_0}, \quad \bar{w} = \frac{w}{u_0}, \quad \bar{p} = \frac{p}{\rho u_0^2},$$
$$\theta = \frac{T-T_1}{T_2-T_1}, \quad \bar{\mu} = \frac{\mu}{\mu_r},$$

https://doi.org/10.1017/S0022377801001313 Published online by Cambridge University Press

$Re = \dfrac{\rho u_0 h}{\mu_r}$ is the Reynolds number,

$\mathbb{S} = \dfrac{\rho v_0 h}{\mu_r}$ is the suction parameter,

$Pr = \dfrac{\rho c_p u_0 h}{k}$ is the Prandtl number,

$Ec = \dfrac{u_0 \mu_r}{\rho c_p h (T_2 - T_1)}$ is the Eckert number,

$Ha^2 = \dfrac{\sigma B_0^2 h^2}{\mu_r}$ is the square of the Hartmann number,

$\mu_r = \dfrac{K u_0^{1-n}}{h^{1-n}}$ is the generalized reference viscosity.

The generalized reference viscosity is chosen here so that when $n = 1$ (Newtonian fluid), the viscosity becomes constant (Kakac et al. 1987; Attia 1998). Here u_0 is the characteristic velocity, which is arbitrarily chosen such that $Re = 1$. Also, in terms of the above non-dimensional variables and parameters, (5)–(7) are written as (where the bars are dropped for convenience)

$$\frac{\partial u}{\partial t} + \mathbb{S}\frac{\partial u}{\partial y} = -\frac{dp}{dx} + \frac{\partial}{\partial y}\left(\mu \frac{\partial u}{\partial y}\right) - \frac{Ha^2}{1+m^2}(u + mw), \tag{10}$$

$$\frac{\partial w}{\partial t} + \mathbb{S}\frac{\partial w}{\partial y} = \frac{\partial}{\partial y}\left(\mu \frac{\partial w}{\partial y}\right) - \frac{Ha^2}{1+m^2}(w - mu), \tag{11}$$

$$\frac{\partial \theta}{\partial t} + \mathbb{S}\frac{\partial \theta}{\partial y} = \frac{1}{Pr}\frac{\partial^2 \theta}{\partial y^2} + Pr\, Ec\, \mu \left[\left(\frac{\partial u}{\partial y}\right)^2 + \left(\frac{\partial w}{\partial y}\right)^2\right] + \frac{Ha^2 Ec}{1+m^2}(u^2 + w^2), \tag{12}$$

where

$$\mu = \left[\left(\frac{\partial u}{\partial y}\right)^2 + \left(\frac{\partial w}{\partial y}\right)^2\right]^{(n-1)/2}. \tag{13}$$

The initial and boundary conditions for the velocity and temperature in dimensionless form are written as

$$u = w = 0 \quad \text{at } t \leqslant 0; \qquad u = w = 0 \quad \text{at } y = \pm 1 \quad \text{for } t > 0; \tag{14}$$

$$\theta = 0 \quad \text{at } t \leqslant 0; \qquad \theta = 0 \quad \text{at } y = -1, \quad \theta = 1 \quad \text{at } y = 1 \quad \text{for } t > 0. \tag{15}$$

3. Numerical solution

Equations (10)–(12) represent a coupled system of nonlinear partial differential equations, which are solved numerically under the initial and boundary conditions (14), using the finite difference approximations. A linearization technique is first applied to replace the nonlinear terms at a linear stage, with the corrections incorporated in subsequent iterative steps until convergence is reached. Then the Crank–Nicolson implicit method (Mitchell and Griffiths 1980) is used at two successive time levels. An iterative scheme is used to solve the linearized system of difference equations. The solution at a certain time step is chosen as an initial guess for next time step, and the iterations are continued until convergence, within a prescribed accuracy. Finally, the resulting block tridiagonal system is solved using the

https://doi.org/10.1017/S0022377801001313 Published online by Cambridge University Press

generalized Thomas algorithm (Mitchell and Griffiths 1980). The energy equation (12) is a linear inhomogeneous second-order ordinary differential equation whose right-hand side is known from the solutions of the flow equations (10), (11), and (13). The values of the velocity components are substituted in the right-hand side of (12), which is solved numerically with the initial and boundary conditions (15) using central differences for the derivatives and the Thomas algorithm for the solution of the set of discritized equations. Finite difference equations relating the variables are obtained by writing the equations at the midpoint of the computational cell and then replacing the different terms by their second-order central difference approximations in the y direction. The diffusion terms are replaced by the average of the central differences at two successive time levels. The computational domain is divided into meshes each of dimension Δt and Δy in time and space respectively as shown in Fig. 2. We define the variables $v = u_y$, $B = w_y$, $H = \theta_y$, and $\mu' = \mu_y$ to reduce the second-order differential equations (10)–(12) to first-order differential equations. The finite difference representations for the resulting first-order differential equations (10) and (11) take the forms

$$\begin{aligned}
&\frac{u_{i+1,j+1} - u_{i,j+1} + u_{i+1,j} - u_{i,j}}{2\Delta t} + \mathbb{S}\frac{v_{i+1,j+1} + v_{i,j+1} + v_{i+1,j} + v_{i,j}}{4} \\
&\quad = -\frac{dp}{dx} + \frac{\bar{\mu}_{i,j+1} + \bar{\mu}_{i,j}}{2}\frac{v_{i+1,j+1} + v_{i,j+1} - (v_{i+1,j} + v_{i,j})}{2\Delta y} \\
&\qquad + \frac{\bar{\mu}'_{i,j+1} + \bar{\mu}'_{i,j}}{2}\frac{v_{i+1,j+1} + v_{i,j+1} + v_{i+1,j} + v_{i,j}}{4} - \frac{Ha^2}{1+m^2} \\
&\qquad \times \left(\frac{u_{i+1,j+1} + u_{i,j+1} + u_{i+1,j} + u_{i,j}}{4} + m\frac{w_{i+1,j+1} + w_{i,j+1} + w_{i+1,j} + w_{i,j}}{4} \right), \quad (16)
\end{aligned}$$

$$\begin{aligned}
&\frac{w_{i+1,j+1} - w_{i,j+1} + w_{i+1,j} - w_{i,j}}{2\Delta t} + \mathbb{S}\frac{B_{i+1,j+1} + B_{i,j+1} + B_{i+1,j} + B_{i,j}}{4} \\
&\quad = \frac{\bar{\mu}_{i,j+1} + \bar{\mu}_{i,j}}{2}\frac{B_{i+1,j+1} + B_{i,j+1} - (B_{i+1,j} + B_{i,j})}{2\Delta y} \\
&\qquad + \frac{\bar{\mu}'_{i,j+1} + \bar{\mu}'_{i,j}}{2}\frac{B_{i+1,j+1} + B_{i,j+1} + B_{i+1,j} + B_{i,j}}{4} + \frac{Ha^2}{1+m^2} \\
&\qquad \times \left(m\frac{u_{i+1,j+1} + u_{i,j+1} + u_{i+1,j} + u_{i,j}}{4} - \frac{w_{i+1,j+1} + w_{i,j+1} + w_{i+1,j} + w_{i,j}}{4} \right). \quad (17)
\end{aligned}$$

The variables with bars are given initial guesses from the previous time steps, and an iterative scheme is used at every time to solve the linearized system of difference equations. Then the finite difference form for the energy equation (12) can be written as

$$\begin{aligned}
&\frac{\theta_{i+1,j+1} - \theta_{i,j+1} + \theta_{i+1,j} - \theta_{i,j}}{2\Delta t} + \mathbb{S}\frac{H_{i+1,j+1} + H_{i,j+1} + H_{i+1,j} + H_{i,j}}{4} \\
&\qquad = \frac{1}{Pr}\frac{H_{i+1,j+1} + H_{i,j+1} - (H_{i+1,j} + H_{i,j})}{2\Delta y} + DISP, \quad (18)
\end{aligned}$$

where $DISP$ represents the Joule and viscous dissipation terms, which are known from the solution of the momentum equations and can be evaluated at the midpoint (i, j) of the computational cell. Computations have been made for $dp/dx = 5$, $Pr = 1$, and $Ec = 0.2$. Grid-independence studies show that the computational domain $0 < t < \infty$ and $-1 < y < 1$ can be divided into intervals with step sizes $\Delta t = 0.0001$ and $\Delta y = 0.005$ for time and space, respectively. Smaller step sizes do not show any

https://doi.org/10.1017/S0022377801001313 Published online by Cambridge University Press

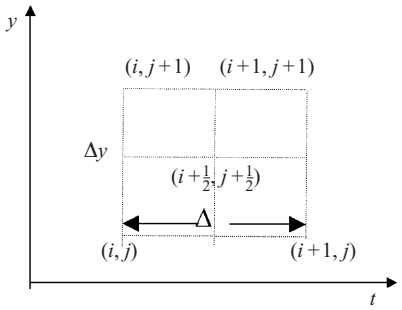

Figure 2. Mesh network.

significant change in the results. Convergence of the scheme is assumed when any one of u, v, w, B, θ, and H for the last two approximations differs from unity by less than 10^{-6} for all values of y in $-1 < y < 1$ at every time step. Fewer than seven approximations are required to satisfy this convergence criteria for all ranges of the parameters studied here. In order to examine the accuracy and correctness of the solutions, the results for the non-magnetic and Newtonian cases are compared and shown to have complete agreement with those reported by Attia (1998). This ensures the satisfaction of all the governing equations; mass continuity, momentum and energy equations.

4. Results and discussion

Figures 3, 4, and 5 show the time development profiles of the velocity components u and w, and the temperature θ, respectively, for various values of time t and for $n = 0.5$ (pseudoplastic or shear-thinning fluid), 1.0 (Newtonian fluid), and 1.5 (dilatant or shear-thickening fluid). The figures are plotted for $Ha = 3$, $m = 3$, and $\mathbb{S} = 1$. As shown in the figures, the profiles are asymmetric about the plane $y = 0$ because of the suction. It is clear from Figs 3 and 4 that increasing the flow index n, which increases the viscosity, decreases the velocity components u and w and the time at which they reach their steady state values. The figures show also that the velocity components u and w do not reach their steady state monotonically. Both u and w increase with time up till a maximum value, and then decrease up to the steady state. This behavior is more pronounced for small values of the parameter n, and it is more clear for u than for w. Figures 3(a) and 4(a) indicate that small values of n affect the parabolic shape of the velocity profile and lead to the suppression of the peaks. This may be due to the increase in the velocities and their steady state times as a result of decreasing n. Figure 5 shows that the temperature profile reaches its steady state monotonically. It is observed also that the velocity component u reaches the steady state faster than w, which, in turn, reaches the steady state faster than θ. This is expected, since u is the source of w, while both u and w act as sources for the temperature.

Figures 6, 7, and 8 show the effect of the Hall parameter m on the time development of u, w, and θ, respectively, at the center of the channel ($y = 0$) for various values of the Hall parameter m and for $n = 0.5$, 1.0 and 1.5. In these figures, $Ha = 3$ and $\mathbb{S} = 1$. Figure 6 shows that u increases with increasing m for all values of n as the effective conductivity ($= \sigma/(1 + m^2)$) decreases with increasing m, which reduces the magnetic damping force on u. It is also observed from the figure that

https://doi.org/10.1017/S0022377801001313 Published online by Cambridge University Press

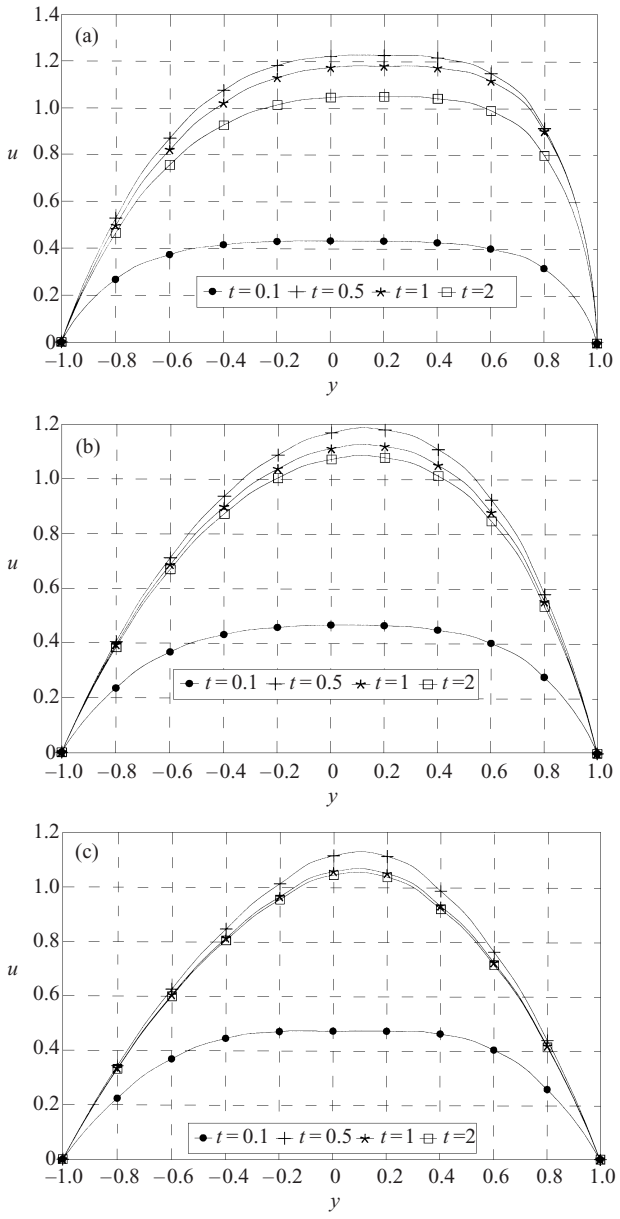

Figure 3. Time development of the velocity component u: (a) $n = 0.5$; (b) $n = 1.0$; (c) $n = 1.5$.

the time at which u reaches its steady state value increases with increasing m while it decreases when n increases. In Fig. 7, the velocity component w increases with increasing m, since w is a result of the Hall effect. On the other hand, at small times, w decreases when m increases. This happens because at small times, w is very small, and then the source term of w is proportional to $mu/(1 + m^2)$, which decreases with increasing m ($m > 1$). This accounts for the crossing of the curves of w with t for all values of n. However, Fig. 7(c) indicates that for large values of

https://doi.org/10.1017/S0022377801001313 Published online by Cambridge University Press

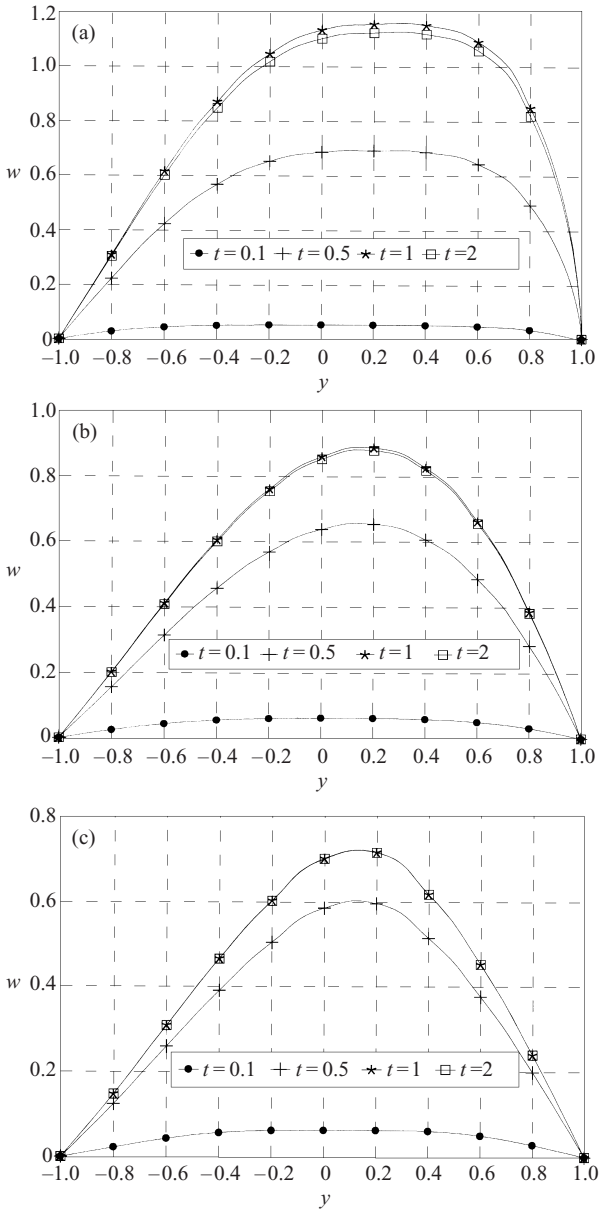

Figure 4. Time development of the velocity component w: (a) $n = 0.5$; (b) $n = 1.0$; (c) $n = 1.5$.

n ($n = 1.5$) and m ($m > 3$), increasing m decreases w for all values of time t, with suppression of the crossing of the curves. This is because large values of n decrease u and w more for all values of t, and, at the same time, large values of m reduce the effective conductivity. Hence, large values of n and m decrease the source term of w and, in turn, decrease w for all values of t. The time at which w reaches the steady state increases with the large increase in m and large decrease in n. Figures 6 and 7 indicate also how the influence of n on u and w depends on m. Increasing n, which increases the viscosity, decreases u and w if m is large ($m > 3$). This is expected,

https://doi.org/10.1017/S0022377801001313 Published online by Cambridge University Press

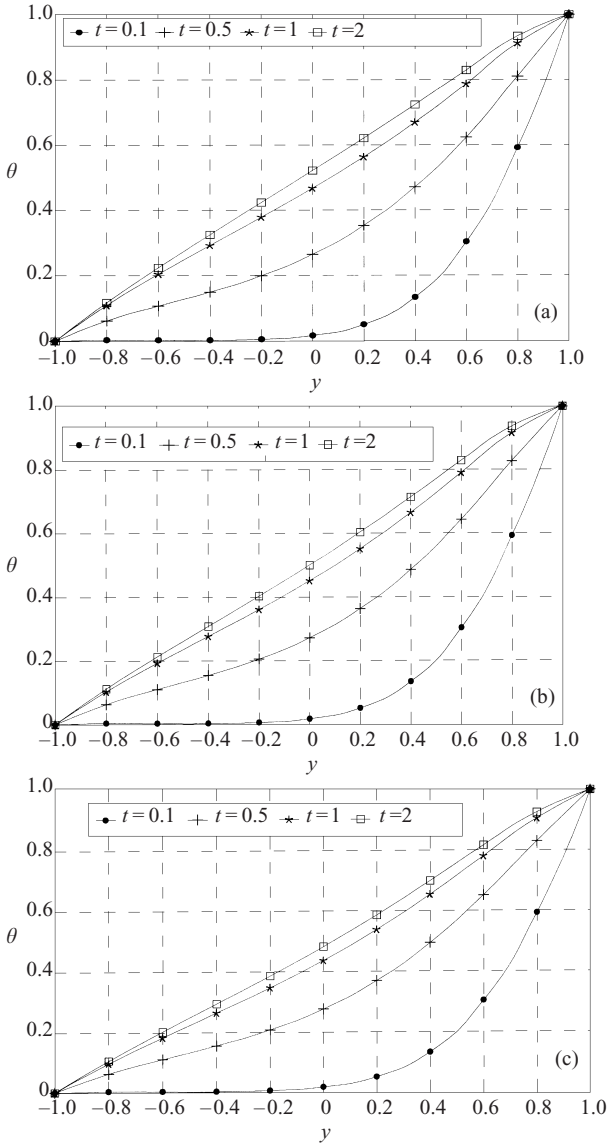

Figure 5. Time development of the temperature profile θ: (a) $n = 0.5$; (b) $n = 1.0$; (c) $n = 1.5$.

since large values of m increase u and w more, which results in a pronounced effect of n on u and w. However, in the case of small m ($0 < m < 3$), changing n has no significant effect on u or w, because all of them are already very small because of the large damping force ($Ha = 3$), and any variation in n cannot change u or w significantly. An interesting phenomenon is observed in Figs 6 and 7, namely, when m is non-zero, the components u and, sometimes, w overshoot. For some times, they exceed their steady state values and then go down towards steady state. The time at which overshooting occurs decreases with increasing n. Increasing m decreases θ at small times and increases it at large times. This is due to the fact that, for small times, u and w are small and an increase in m increases u but decreases w.

https://doi.org/10.1017/S0022377801001313 Published online by Cambridge University Press

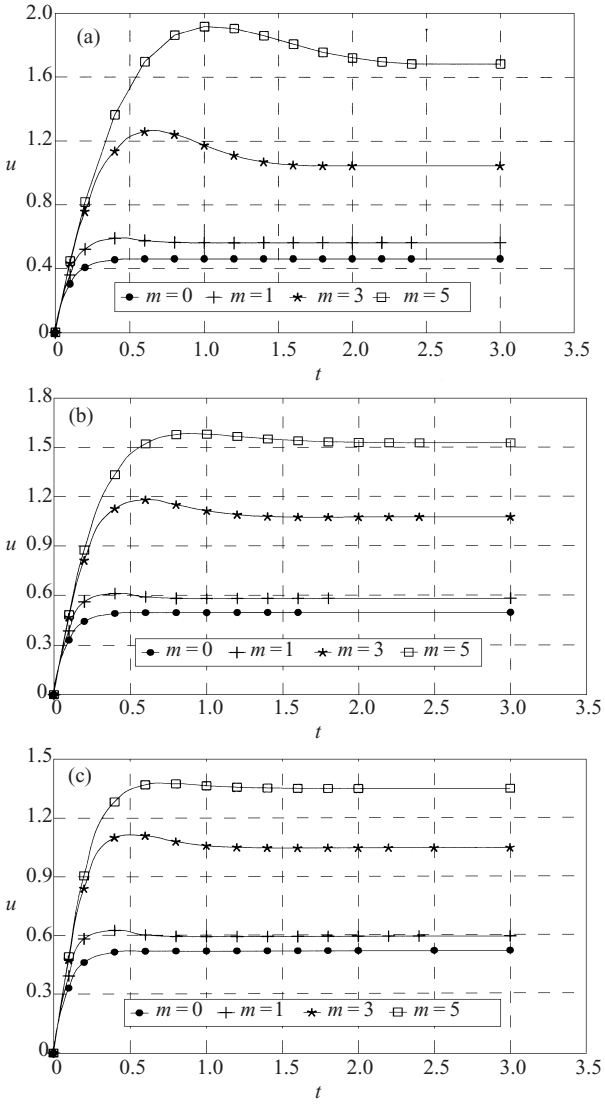

Figure 6. Effect of the Hall parameter m on the time development of u at $y = 0$: (a) $n = 0.5$; (b) $n = 1.0$; (c) $n = 1.5$.

Then, the Joule dissipation, which is also proportional to $(1+m^2)^{-1}$, decreases. For large times, increasing m increases both u and w, and, in turn, increases the Joule and viscous dissipations. This accounts for the crossing of the curves of θ with time for all values of n. It is also observed that increasing n decreases θ for all non-zero values of m. This is because increasing n, when m is not zero, decreases both u and w and their gradients which decreases the Joule and viscous dissipations. In the case $m = 0$, increasing n increases θ as a result of increasing the viscous dissipation. Figure 8 shows also that the time at which θ reaches its steady state value increases with increasing m, while it is not greatly affected by changing n.

Figures 9, 10, and 11 show the effect of the Hartmann number Ha on the time development of u, w, and θ, respectively, at $y = 0$ with time for various values

https://doi.org/10.1017/S0022377801001313 Published online by Cambridge University Press

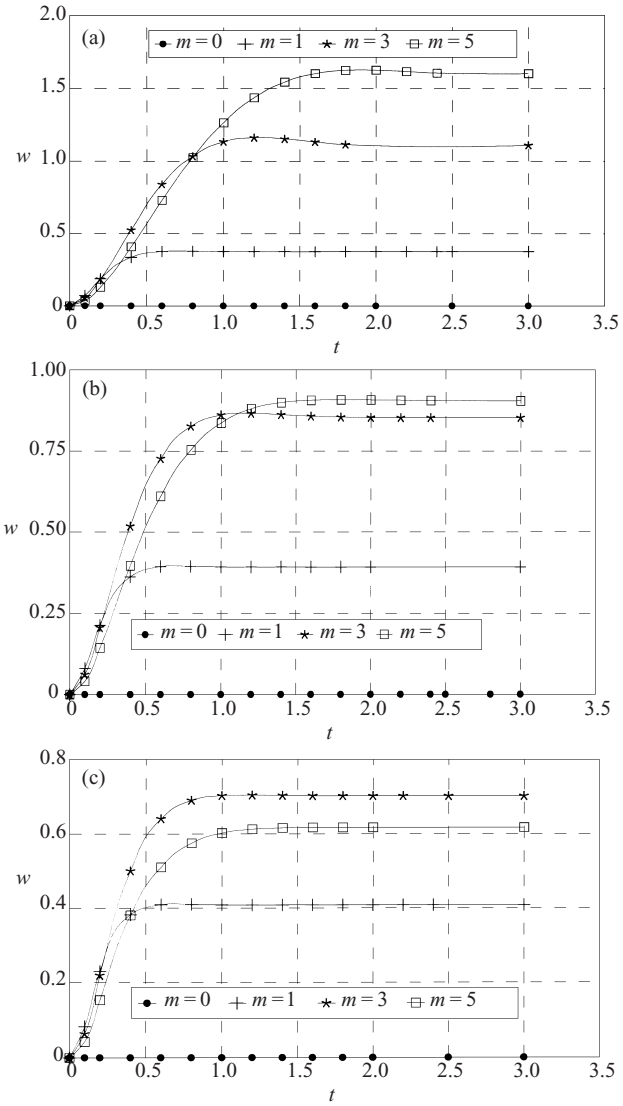

Figure 7. Effect of the Hall parameter m on the time development of w at $y = 0$: (a) $n = 0.5$; (b) $n = 1.0$; (c) $n = 1.5$.

of Ha and for $n = 0.5$, 1.0, and 1.5. In these figures, $m = 3$ and $\mathbb{S} = 1$. Figure 9 shows that increasing Ha decreases u, since it increases the damping force on u. On the other hand, Fig. 10 indicates that increasing Ha increases w, since it increases the source term of w, which is proportional to Ha^2u for various values of n. It is also clear from Figs 9 and 10 that u and w overshoot for large values of Ha when the Hall effect is considered ($m = 3$). The overshooting in u and w decreases with increasing n due to the decreases in both u and w. It should be pointed out that although the Hall effect is considered ($m = 3$), the overshooting in u and w appears only when Ha is large ($Ha = 3$). This emphasizes the fact that the Hall effect becomes more pronounced in the case that the magnetic field is high. Figure 10(a) presents an interesting phenomenon, which is the appearance of the crossing

https://doi.org/10.1017/S0022377801001313 Published online by Cambridge University Press

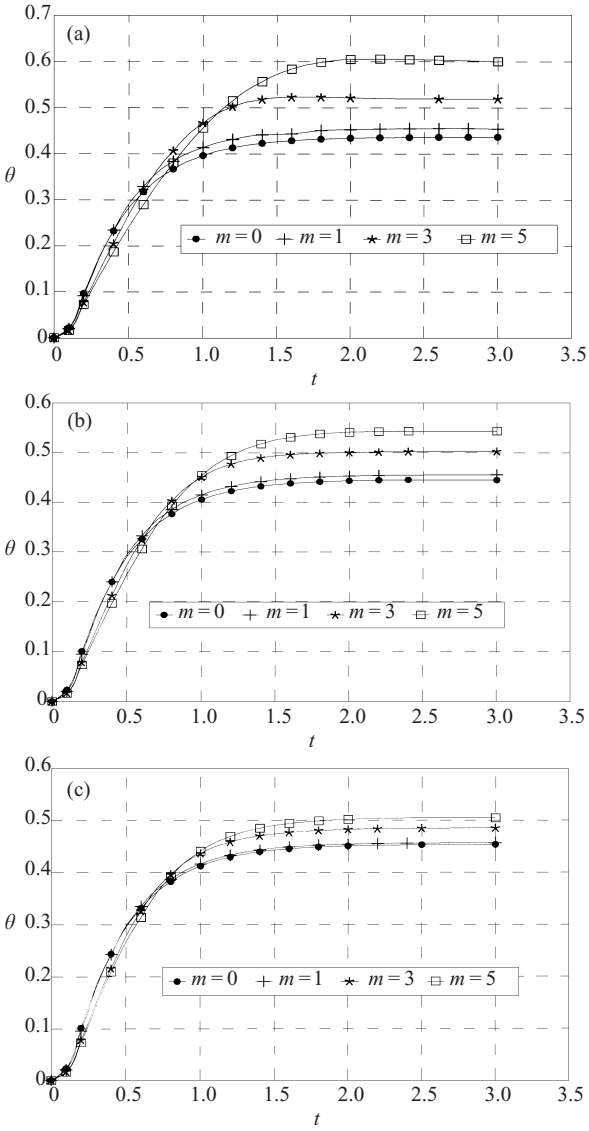

Figure 8. Effect of the Hall parameter m on the time development of θ at $y = 0$: (a) $n = 0.5$; (b) $n = 1.0$; (c) $n = 1.5$.

of w curves with time for large values of Ha and small values of n. Increasing Ha increases w for small t and decreases w for large t when n is small ($n = 0.5$). This is because for small t, w is small and increasing Ha increases the source term of w and then increases w for all values of n. Small values of n increase w more; then, with the progress of time, the resulting large increase in w decreases u more since it increases the damping force on u. Hence, the large decrease in u as well as the large increase in w decrease greatly the source term of w which reduces w more and results in the crossing appears in the figure. Figure 11 shows that the effect of Ha on the temperature θ depends on t. In the case of large Ha, for small values of t, the velocity components u and w are small, and increasing Ha, although it decreases

https://doi.org/10.1017/S0022377801001313 Published online by Cambridge University Press

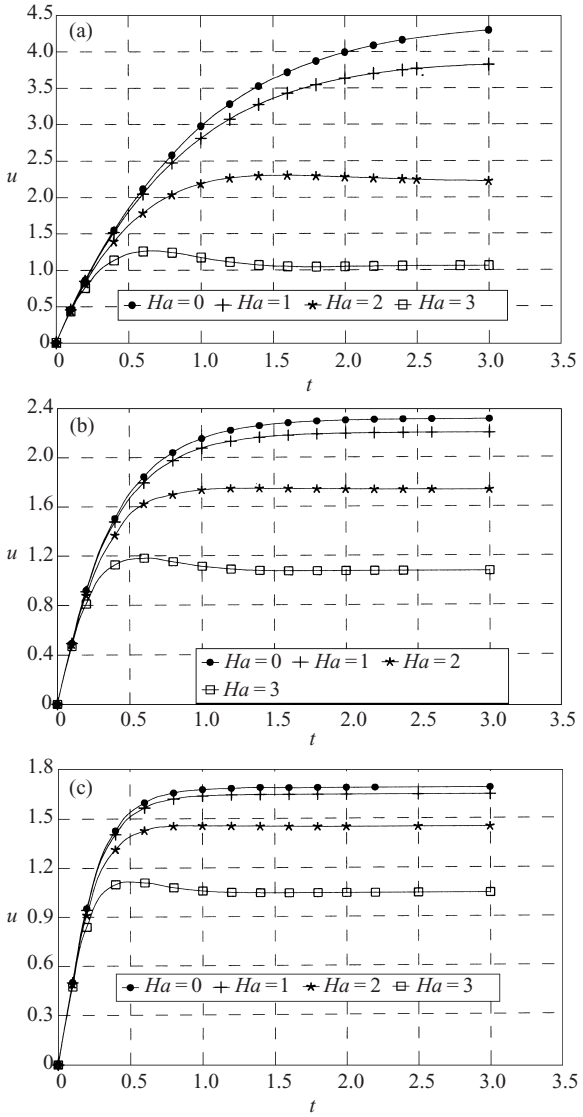

Figure 9. Effect of the Hartmann number Ha on the time development of u at $y = 0$: (a) $n = 0.5$; (b) $n = 1.0$; (c) $n = 1.5$.

u and w and their gradients, increases the Joule dissipations and then increases θ. However, for large values of t, increasing Ha decreases θ due to the reduction in the Joule and viscous dissipations. If Ha is small ($0 < Ha < 1$), then increasing Ha increases θ for all values of t as a result of increasing the Joule dissipation. Figure 11 also shows that the influence of Ha on θ becomes more pronounced for the case of small n ($n = 0.5$) due to the increase in the velocity components and their gradients, which results in increasing the Joule and viscous dissipations.

Figures 12, 13, and 14 show the effect of the suction parameter $\mathbb{S}$ on the time development of u, w, and θ, respectively, at $y = 0$ with time for various values of the suction $\mathbb{S}$ and for $n = 0.5$, 1.0 and 1.5. In these figures, $Ha = 3$ and $m = 3$.

https://doi.org/10.1017/S0022377801001313 Published online by Cambridge University Press

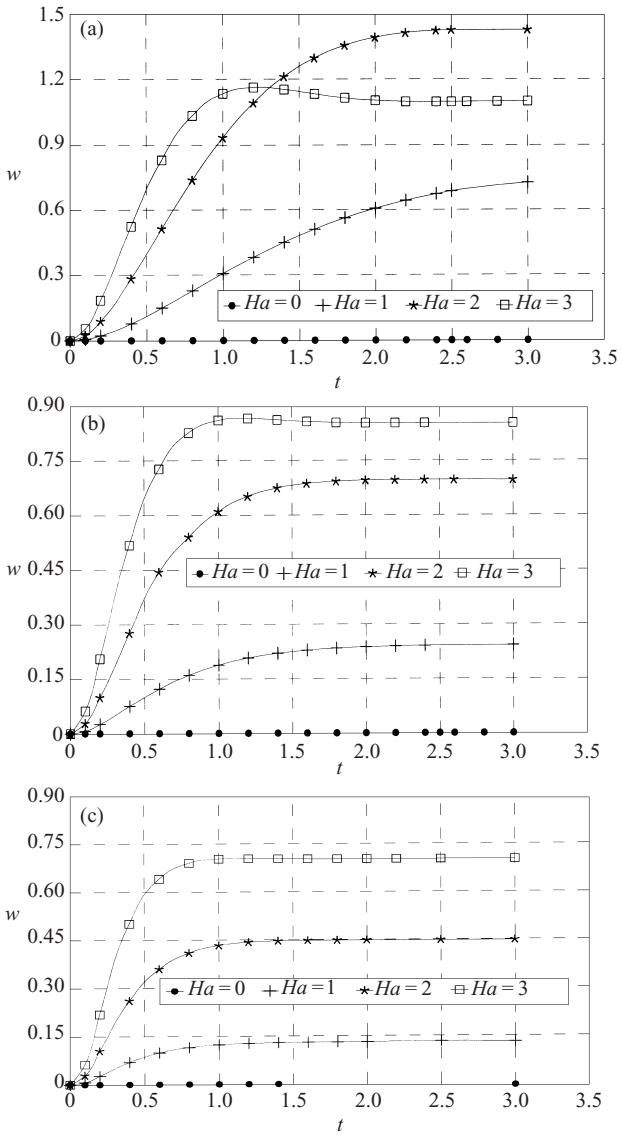

Figure 10. Effect of the Hartmann number Ha on the time development of w at $y = 0$: (a) $n = 0.5$; (b) $n = 1.0$; (c) $n = 1.5$.

Figure 12 shows that u at the center decreases with increasing $\mathbb{S}$ for moderate and high values of n due to the convection of the fluid from regions in the lower half to the center, which has higher fluid speed. However, for small values of n as shown in Fig. 12(a), the velocity component u decreases with increasing $\mathbb{S}$ for some time, and then increases as time develops. The increase in u that occurs during the progress of time, as a result of increasing $\mathbb{S}$, may be due to the suppression of the peaks of the profiles of u shown in Fig. 3(a) for small values of n. Figure 13 shows that w decreases with increasing $\mathbb{S}$ for all values of n as a result of decreasing u, which affects the source term of w. Figure 13 also shows the influence of $\mathbb{S}$ on the reduction of the overshooting in w, especially for small values of n ($n = 0.5$). It is

https://doi.org/10.1017/S0022377801001313 Published online by Cambridge University Press

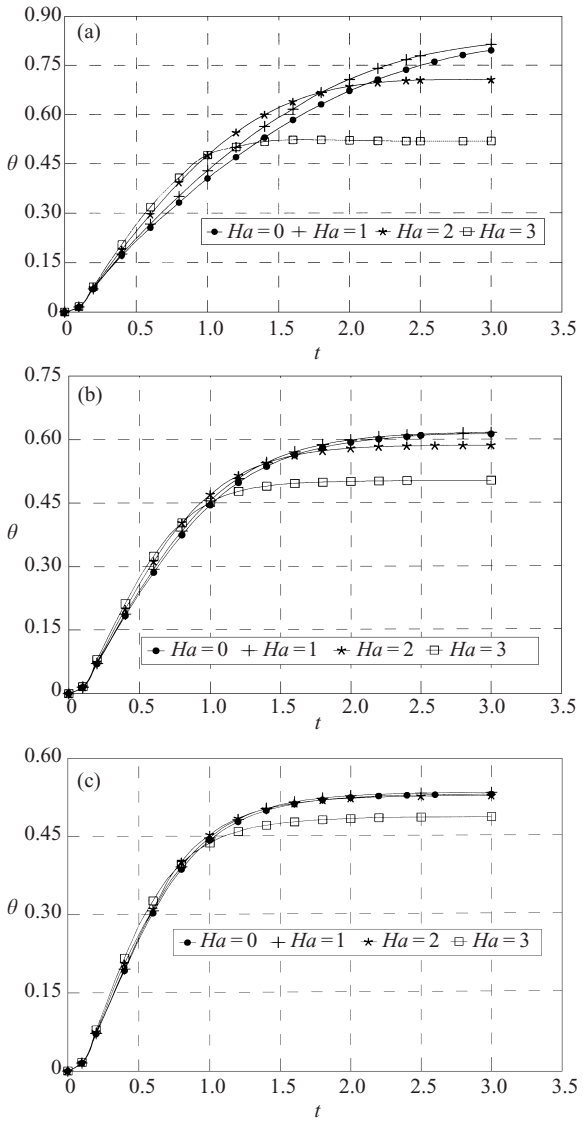

Figure 11. Effect of the Hartmann number Ha on the time development of θ at $y = 0$: (a) $n = 0.5$; (b) $n = 1.0$; (c) $n = 1.5$.

clear from Figs 12 and 13 that the influence of $\mathbb{S}$ on u and w is more pronounced for the case of small n due to the decreases in both u and w. It is also apparent from the figures that the effect of $\mathbb{S}$ on w is more pronounced than that on u, especially for moderate and large values of n. Figure 14 indicates that increasing $\mathbb{S}$ decreases the temperature at the center of the channel for all values of n. This is due to the influence of convection in pumping the fluid from the cold lower half towards the center of the channel.

Tables 1–6 present the steady state value of the temperature θ at the center of the channel for various values of m and n and for $\mathbb{S} = 0$. In Tables 1–3, $Ha = 3$, while in Tables 4–6, $Ha = 10$. In Tables 1 and 4, both the viscous and Joule

https://doi.org/10.1017/S0022377801001313 Published online by Cambridge University Press

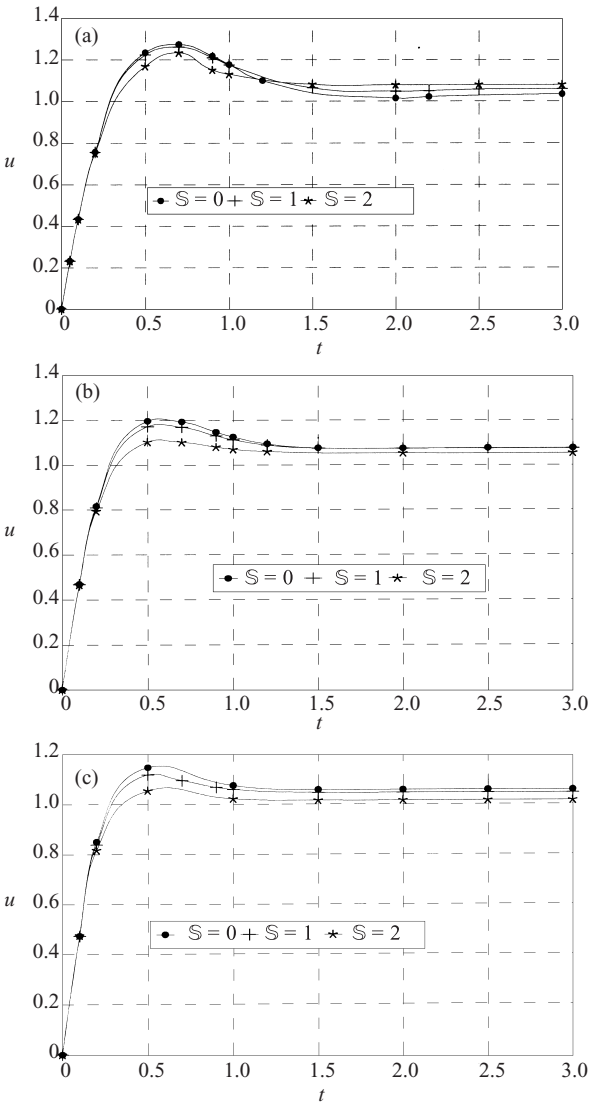

Figure 12. Effect of the suction parameter $\mathbb{S}$ on the time development of u at $y = 0$: (a) $n = 0.5$; (b) $n = 1.0$; (c) $n = 1.5$.

dissipations are taken into consideration. In Tables 2 and 5, the viscous dissipation is not considered, while the Joule dissipation is neglected in the calculations of Tables 3 and 6. Comparing Tables 2 and 3 with Table 1 indicates that both the viscous and Joule dissipations have a reasonable effect on θ. The viscous dissipation has an apparent effect on θ for larger values of m and n. On the other hand, the effect of the Joule dissipation on θ becomes more pronounced for small values of m and n. Also, Table 1 shows that the variation of θ with n depends on m. Increasing n decreases θ for small m, while it increases θ for large m. Such behavior is not greatly affected by the viscous dissipation, as shown in Table 2. However, Table 3 indicates that the Joule dissipation is the main reason for such behavior.

For large values of the magnetic field ($Ha = 10$), and by comparing Tables 4

https://doi.org/10.1017/S0022377801001313 Published online by Cambridge University Press

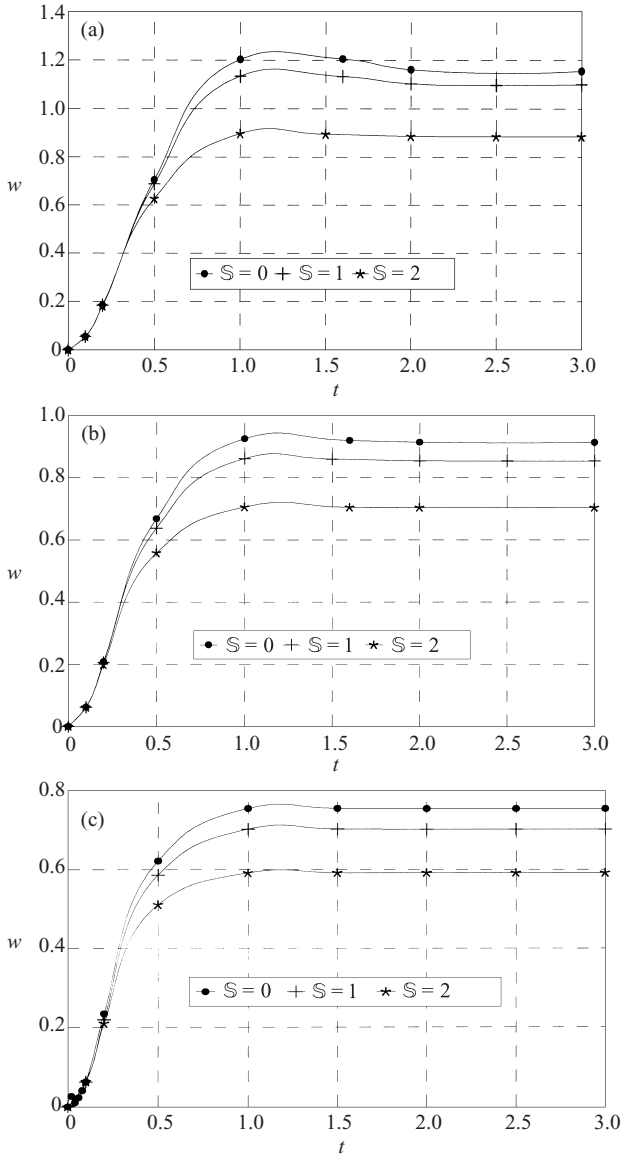

Figure 13. Effect of the suction parameter $\mathbb{S}$ on the time development of w at $y = 0$: (a) $n = 0.5$; (b) $n = 1.0$; (c) $n = 1.5$.

Table 1. The steady state temperature θ at the center of the channel for various values of m and n with viscous and Joule dissipations ($Ha = 3$).

n	$m = 0$	$m = 1$	$m = 3$	$m = 5$
0.5	0.6830	0.7048	0.7769	0.8692
1.0	0.6966	0.7073	0.7631	0.8160
1.5	0.7057	0.7086	0.7439	0.7696

https://doi.org/10.1017/S0022377801001313 Published online by Cambridge University Press

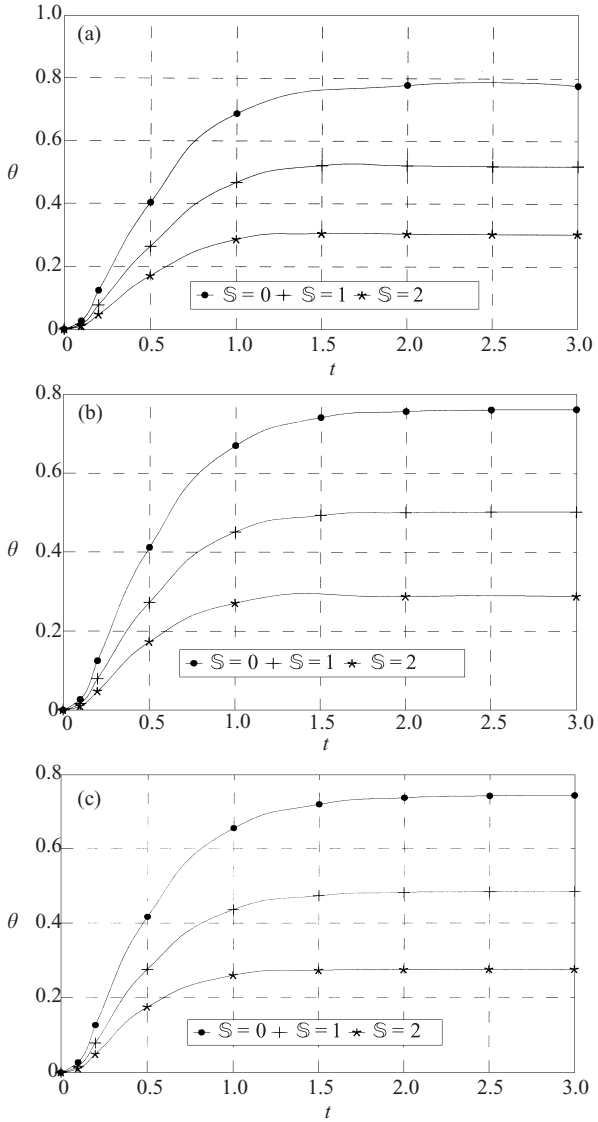

Figure 14. Effect of the suction parameter $\mathbb{S}$ on the time development of θ at $y = 0$: (a) $n = 0.5$; (b) $n = 1.0$; (c) $n = 1.5$.

Table 2. The steady state temperature θ at the center of the channel for various values of m and n with Joule dissipation ($Ha = 3$).

n	$m = 0$	$m = 1$	$m = 3$	$m = 5$
0.5	0.6707	0.6809	0.6839	0.6756
1.0	0.6827	0.6771	0.6334	0.5879
1.5	0.6922	0.6761	0.6038	0.5553

https://doi.org/10.1017/S0022377801001313 Published online by Cambridge University Press

Table 3. The steady state temperature θ at the center of the channel for various values of m and n with viscous dissipation ($Ha = 3$).

n	$m = 0$	$m = 1$	$m = 3$	$m = 5$
0.5	0.5119	0.5235	0.5926	0.6933
1.0	0.5135	0.5299	0.6293	0.7278
1.5	0.5131	0.5320	0.6396	0.7139

Table 4. The steady state temperature θ at the center of the channel for various values of m and n with viscous and Joule dissipations ($Ha = 10$).

n	$m = 0$	$m = 1$	$m = 3$	$m = 5$
0.5	0.5219	0.5232	0.5267	0.5306
1.0	0.5239	0.5241	0.5261	0.5299
1.5	0.5242	0.5243	0.5255	0.5287

Table 5. The steady state temperature θ at the center of the channel for various values of m and n with Joule dissipation ($Ha = 10$).

n	$m = 0$	$m = 1$	$m = 3$	$m = 5$
0.5	0.5217	0.5226	0.5239	0.5244
1.0	0.5237	0.5238	0.5242	0.5245
1.5	0.5242	0.5241	0.5240	0.5241

and 5, it is seen that the influence of the viscous dissipation on θ can be neglected. However, as shown in Table 6, the Joule dissipation is still effective on θ, although it has a more pronounced effect for small values of Ha.

5. Conclusions

The transient Hartmann flow of a power-law non-Newtonian fluid under the influence of an applied uniform magnetic field has been studied, considering the Hall effect. The effects of the non-Newtonian fluid behavior (flow index n), the magnetic field (Hartmann number Ha), the Hall effect (Hall parameter m), and the suction or injection velocity (suction parameter $\mathbb{S}$) have been investigated. The Hall term affects the main velocity component u in the x direction and gives rise to another velocity component w in the z direction. An overshooting in the velocity components u and w with time due to the Hall effect is observed for all values of n and high values of the magnetic field. The non-Newtonian characteristics have an apparent effect in controlling the overshooting in u or w and the time at which it occurs. The results show that the influence of the parameter n on u and w depends on the Hall current. When m is large, increasing n decreases u and w, but when m is small, the parameter n has no significant effect on u or w. It is found also that the effect of the Hall term on w depends on time and the non-Newtonian characteristics. Unless n is large, increasing m decreases w when t is small but increases it when t is large. It is observed that the variation of w with the magnetic field depends on the non-Newtonian characteristics and time. For small values of n and large values of Ha, increasing Ha increases w for small t, and decreases w for large t. This results in a crossover of the (w, t) graph for different values of Ha, provided that the Hall effect is considered, Ha is large, and n is small. The dependence of u on the suction velocity is shown to vary with the non-Newtonian characteristics and time. If n is small, increasing $\mathbb{S}$ decreases u for some time and then increases it

https://doi.org/10.1017/S0022377801001313 Published online by Cambridge University Press

Table 6. The steady state temperature θ at the center of the channel for various values of m and n with viscous dissipation ($Ha = 10$).

n	$m = 0$	$m = 1$	$m = 3$	$m = 5$
0.5	0.4999	0.5002	0.5023	0.5059
1.0	0.4997	0.4999	0.5015	0.5050
1.5	0.4997	0.4998	0.5011	0.5042

as time develops. This leads to a crossover of the (u, t) graph for various values of $\mathbb{S}$ in the case of small n. It is also found that the behavior of θ for different values of m or Ha depends only on t. When t is small, θ decreases with increasing m, but when t is large, θ increases with increasing m. On the other hand, increasing the magnetic field increases θ for small t and decreases it for large t. The effect of the Hall term or the magnetic field on the magnitude of θ depends on the characteristics of the non-Newtonian fluid, and becomes more pronounced in case of small n. The time at which u reaches its steady state increases with increasing m, but decreases when n increases. The same conditions are valid for w; however, only large values of m and n have significant effects on the steady state times of w. The time at which θ reaches its steady state increases with increasing Hall current, while it is not greatly affected by changing the characteristics of the non-Newtonian fluid.

Viscous dissipation has an apparent effect on the temperature for larger values of m and n and for smaller values of Ha. However, Joule dissipation has a marked effect on the temperature for smaller values of m, n, and Ha. In general, it is observed that Joule dissipation has a more pronounced effect on θ than viscous dissipation.

References

Alpher, R. A. 1961 *Int. J. Heat Mass Transfer* **3**, 108.

Attia, H. A. 1998 *Can. J. Phys.* **76**, 739.

Attia, H. A. and Kotb, N. A. 1996 *Acta Mech.* **117**, 215.

Crammer, K. R. and Pai, S.-I. 1973 *Magnetofluid Dynamics for Engineers and Applied Physicists*. New York: McGraw-Hill.

Gao, S. X. and Hartnett, J. P. 1992 *Int. Commun. Heat Mass Transfer* **19**, 673.

Gingrich, W. K., Cho, Y. I. and Shyy, W. 1992 *Int. J. Heat Mass Transfer* **35**, 2823.

Ibrahim, F. N. and Terbeche, M. 1994 *J. Phys. D: Appl. Phys.* **27**, 740.

Kakac, S., Shah, R. K. and Aung, W. 1987 *Handbook of Single-Phase Convective Heat Transfer*. New York: Wiley.

Metzner, A. B. 1965 *Adv. Heat Transfer* **2**, 357–397.

Mitchell, A. R. and Griffiths, D. F. 1980 *The Finite Difference Method in Partial Differential Equations*. New York: Wiley.

Nakayama, A. and Koyama, H. 1988 *Warme- und Stoffubertragung* **22**, 29.

Nigam, S. D. and Singh, S. N. 1960 *Q. J. Mech. Appl. Maths* **13**, 85.

Patel, N. and Ingham, D. B. 1994 *Int. Commun. Heat Mass Transfer* **21**, 75.

Schlichting, H. 1968 *Boundary Layer Theory*, 6th edn. New York: McGraw-Hill.

Soundalgekar, V. M. and Uplekar, A. G. 1986 *IEEE Trans. Plasma Sci.* **PS-14**, 579–583.

Soundalgekar, V. M., Vighnesam, N. V. and Takhar, H. S. 1979 *IEEE Trans. Plasma Sci.* **PS-7**, 178–182.

Sutton, G. W. and Sherman, A. 1965 *Engineering Magnetohydrodynamics*. New York: McGraw-Hill.

Tani, I. 1962 *J. Aerospace Sci.* **29**, 287.

Tao, I. N. 1960 *J. Aerospace Sci.* **27**, 334.

Tien, C. H. F. 1962 *Can. J. Chem. Engng.* **40**, 130.